Final Report

NARROW BANDGAP SEMICONDUCTING SILICIDES: INTRINSIC INFRARED DETECTORS ON A SILICON CHIP

Principal Investigator: Dr. John E. Mahan
Colorado Research Development Corporation
Drake Creekside Two
Suite 319
2629 Redwing
Fort Collins, CO 80526

Abstract

Polycrystalline thin films of $CrSi_2$, $LaSi_2$, and $ReSi_2$ were grown on silicon substrates. Normal incidence optical transmittance and reflectance measurements were made as a function of wavelength. It was demonstrated that $LaSi_2$ is a metallic conductor, but that $CrSi_2$ and $ReSi_2$ are, in fact, narrow bandgap semiconductors. For $CrSi_2$, the complex index of refraction was determined by computer analysis of the optical data. From the imaginary part, the optical absorption coefficient was determined as a function of photon energy. It was shown that $CrSi_2$ possesses an indirect forbidden energy gap of slightly less than 0.31 eV, and yet it is a very strong absorber of light above the absorption edge. On the other hand, the $ReSi_2$ films exhibit an absorption edge in the vicinity of 0.2 eV. Measurements of the thermal activation energy of resistivity for $ReSi_2$ indicate a bandgap of 0.18 eV. It is concluded that the semiconducting silicides merit further investigation for development as new silicon-compatible infrared detector materials.

Introduction

In fulfillment of the technical objectives of our Phase I research contract, we have fabricated thin films of $CrSi_2$, $LaSi_2$, and $ReSi_2$, have characterized them structurally and compositionally, have measured the optical transmittance and reflectance, and have obtained optical constants from the data where the materials lend themselves to the techniques available to us. The details of this experimental work and analysis are presented in the following sections.

Experimental Procedure

Chromium, lanthanum, and rhenium films were deposited onto silicon substrates by neutralized ion beam sputtering from metal targets [1]. Substrates for optical properties measurements were 1-0-0 or 1-1-1 orientation, polished silicon wafers [2]. Metal films were also deposited onto similar wafers which were previously thermally oxidized and coated with undoped polycrystalline silicon (polysilicon) by low pressure chemical vapor deposition. (The polysilicon substrates were unsuitable for optical characterization; the purpose of these was to electrically isolate the silicide film from the silicon substrate to allow accurate resistivity measurements.) All substrates were ion milled within the vacuum chamber immediately prior to deposition, in order to obtain clean metal-silicon interfaces.

The silicide layers were formed by heating the samples in a quartz tube furnace under high purity flowing argon. In each case, the metal film was completely consumed by the substrate in forming the disilicide. The growth conditions were 120 minutes at 1100 for $CrSi_2$, 60 minutes at 600 or 900 C for

$LaSi_2$, and 60 minutes at 900 C for $ReSi_2$.

The lanthanum films were susceptible to a tarnishing reaction when exposed to air, such that over a period of a few hours a 5000 A metal film would be converted entirely to lanthanum oxide. This was observed as a continual change in color of the film in reflection until the metal was totally oxidized. Auger analysis of a fully tarnished film showed a mixture of lanthanum and oxygen throughout the film thickness.

The tarnishing reaction was prevented by capping the lanthanum layer with about 300 A of silicon prior to removing the sample from the ion beam deposition system. The silicon layer formed a thin SiO_2 native oxide which served as a diffusion barrier to the further incorporation of oxygen in the film. The silicon cap was also consumed during silicide formation.

The silicide thicknesses were obtained by measuring the metal thicknesses at a step created by masking during deposition. These thicknesses were calculated from density data neglecting strain and assuming bulk densities. Under such assumptions, the ratio of silicide to metal thicknesses is 3.01 for $CrSi_2$, 1.68 for $LaSi_2$, and 2.56 for $ReSi_2$ [3]. The thickest obtainable $ReSi_2$ film was ~800 A, while in the cases of $CrSi_2$ and $LaSi_2$ films of more than a micron thicknesses were obtained with no indication of an upper limit. Rhenium films corresponding to silicide thickness greater than ~800 A peeled off the substrates during annealing.

The normal incidence optical transmittance and reflectance were measured as functions of wavelength using a Perkin-Elmer 337 Grating Infrared Spectrophotometer for the wavelength range from 3 to 25 microns. For wavelengths shorter than 3 microns, an optical bench with infrared source, grating monochromator, order sorting filters, light chopper, and HgCdTe detector was used. The transmittance of a sample was normalized to that of a

bare half of the substrate. The reflectance was obtained with the aid of a Perkin-Elmer specular reflectance accessory.

The complex index of refraction of the film was extracted from the optical data with the aid of a two-layer optical model [4]. The model considered absorption in the silicide film and multiple reflections within both the silicide film and the substrate. Equations for the measured transmission and reflection were derived from the optical model. These depend on (1) the wavelength, (2) the index of refraction, extinction coefficient, and thickness of the silicide film, and (3) the index of refraction and thickness of the substrate. All other quantities being known, the optical constants of the silicide films were determined from these equations and the data.

The determination of the optical constants was a three-step process because of the transcendental nature of the equations, and because they contain periodic functions. First, all physically realistic pairs of the optical constants, which produce calculated transmittances and reflectances within five percent of the measured values, were determined with a grid search. These pairs of n and k were plotted as functions of wavelength. This produced several distinct continuous curves, corresponding to families of mathematically correct solutions [5]. The physically correct family was determined by comparing these solutions with an index of refraction value which was estimated from the interference fringes in the data. The final values of the optical constants were determined by refining this solution with a damped Newton-Raulphson fit routine.

The optical characterization of the $ReSi_2$ thin films was not entirely possible with the techniques available to us because only very thin films could be obtained, as will be discussed below. Thus, to aid in the

interpretation of the optical data high temperature resistivity measurements were made with a vacuum system equipped with a tungsten wire four-point probe and heaters. The resistivity as a function of temperature was calculated from the measured sheet resistance and the film thickness. The intent was to obtain the thermal activation energy of conductivity within the intrinsic regime, which generally is equal to half the forbidden energy gap.

Materials Characterization

X-ray diffraction with copper Kα radiation was used for phase identification of the silicide films. It was found that a few prominent and unique peaks associated with each phase could be used.

A representative pattern for an hexagonal $CrSi_2$ sample is shown in Figure 1. The prominent peaks are labeled with their Miller indices [6] and are listed in Table I as well. In addition, the (003) peak at 42.6^{o} was frequently observed. A so-called forbidden reflection from the single crystal silicon substrate appears at 32.9^{o} alongside other reflections also due to the substrate.

There are two crystal structures for $LaSi_2$, a low temperature tetragonal phase, and a high temperature orthorhombic phase. The two annealing temperatures cited previously gave apparently single-phase films having each of these structures. Representative X-ray diffraction patterns are given in Figure 2. Unique and prominent peaks for each phase are listed in Table I [7]. Some strong reflections from the single crystal 1-0-0 silicon substrate are seen. Our conclusion that $LaSi_2$ is a metallic conductor is based on an examination of samples of both crystal structures.

Finally, a representative pattern for tetragonal $ReSi_2$ is shown in Figure

Table I

Prominent X-ray Diffraction Peaks

Material	Two Theta	Miller Indices
$CrSi_2$	27.2°	101
	40.7	110
	43.3	111
	47.5	200
	50.2	112
$LaSi_2$		
Tetragonal (600C)	21.9	101
	32.4	112
	42.4	200
Orthorhombic (900C)	21.3	010
	28.4	103
	30.6	111
	31.9	005
	47.8	210
$ReSi_2$	40.8	110
	45.8	103
	47.4	112 and 004

3. Unique and prominent X-ray diffraction peaks for this phase are also listed in Table I [8]. Reflections from the single crystal 1-1-1 silicon substrate are apparent.

In summary, for all three semiconducting silicides the X-ray diffraction data indicate that polycrystalline films of the desired compounds were

obtained, with no evidence of other silicide phases or unreacted metal.

Representative Auger spectra are shown for the three materials in Figures 4 - 6. The spectra were obtained after ion milling the samples in order to remove adsorbed impurities. It is found that the impurity levels within the interior of the films are at or below background levels for the instrument. Peaks for silicon and the respective metals are prominent.

SEM top views and fracture cross-sections are shown in Figures 7 - 9. These approximately confirm the thickness estimates from metal film thicknesses as discussed above. In all cases, there is a sharp interface between silicide film and silicon substrate. The top views show that surface roughness of the $CrSi_2$, while certainly observable, may be presumed to not greatly influence the optical properties since it is of a much smaller size range than the optical wavelengths of interest [9]. Microcracks were sometimes observed in the thickest $CrSi_2$ films, as shown in the left hand side of Figure 7(a). The $LaSi_2$ films are quite rough and of a nonuniform thickness but this is not an issue for optical characterization since the material is not a semiconductor. The $ReSi_2$ film thickness seems to be of sufficient uniformity for optical characterization.

Optical Properties Measurements, Analysis, and Discussion

The optical properties of four $CrSi_2$ films of four different thicknesses are shown in Figure 10. The onset of strong absorption depends on film thickness, moving to lower photon energy for thicker films. Interference fringes, due to multiple internal reflections within the silicide layer are also seen. The real part (n) of the complex index may be estimated from the positions of adjacent extrema in the reflectance spectra using the following equation [10]:

$$n = \frac{\lambda_1 \lambda_2}{2d(\lambda_1 - \lambda_2)}. \qquad (1)$$

λ_1 and λ_2 are the wavelengths corresponding to adjacent reflectance minima and d is the film thickness. The value obtained for n is ~7.5.

The optical absorption coefficient (α), calculated from

$$\alpha = 4\pi k/\lambda , \qquad (2)$$

is shown in Figure 11. k is the imaginary part of the complex index. There is a very strong absorption edge in the vicinity of 0.3 eV which is due to interband transitions, with very high values of the absorption coefficient observed above the edge.

In addition, for photon energies below ~0.2 eV there is an increase in absorption coefficient with decreasing photon energy. The energy dependence here is like that expected for free carrier absorption, and the magnitude and energy range is consistent with that interpretation. An alternative explanation of the sub-bandgap absorption is diffuse scattering due to surface roughness. We are unsure which interpretation is correct; fortunately the phenomenon does not interfere with our determination of the value and type of forbidden energy gap in this material.

The absorption coefficient data are replotted in Figure 12 in a manner that would yield a linear plot for indirect transitions. Actually two linear regimes are predicted, with the two intercepts being the value of the forbidden energy gap (E_g) plus or minus the energy of the phonon (E_p) required for k-conservation [11]:

$$\{\alpha\}^{1/2} = C(h\nu - E_g \pm E_p). \quad (3)$$

C is a constant depending on the details of the band structure, ν is the photon frequency, and h is Planck's constant.

The excellent linear behavior of the data in Figure 12 suggests strongly that the gap is indirect. Only the phonon emission part of the curve is seen however, with an intercept of 0.31 eV. It is necessary, generally, to work with bulk samples if one is to observe the phonon absorption branch. For example, the absorption coefficient within the phonon absorption range is on the order of 10 cm^{-1} or lower for silicon and germanium. We conclude that the indirect gap of $CrSi_2$ is slightly less than 0.31 eV by an amount equal to E_p. This phonon energy is typically a few hundredths of an eV.

There may be direct transitions in $CrSi_2$ at higher energies. Figure 13 shows the data for one sample plotted in a manner appropriate for direct transitions, with the scale chosen to display the behavior well above the fundamental edge. For direct transitions, we have [11]

$$\{\alpha\}^2 = D(h\nu - E_d). \quad (4)$$

D is another constant that depends on the band structure and E_d is the minimum direct gap. The value of E_d from Figure 13 appears to be on the order of 0.57 eV.

All of the $LaSi_2$ films were found to be opaque. That is, there was no measurable transmittance at any wavelength accessible to us for even the thinnest films (~900 A). This behavior is characteristic of the as-deposited metal films and of well-known metallically conducting silicides ($TiSi_2$, $MoSi_2$, $TaSi_2$, and WSi_2) we have made in other research. From sheet resistance

measurements of $LaSi_2$ films formed on polysilicon substrates, we obtain room temperature resistivities of 44 and 81 micro-ohm-cm for the tetragonal and orthorhombic phases, respectively. The resistivity of representative samples of the two $LaSi_2$ phases is shown as a function of temperature in Figure 14. The linear behavior is typical of metallically conducting materials.

Some optical data for $ReSi_2$ are shown in Figure 15. There is an absorption edge in the vicinity of 0.2 eV. We have obtained no clear energy dependence of the optical absorption coefficient for this material, because the previously mentioned difficulties with film fabrication prevented our obtaining films with sufficiently strong absorption. To our knowledge, there is no report in the scientific literature of the formation of $ReSi_2$ thin films by any means [12].

Our problem specifically is that the computer is unable to find solutions to the expressions for reflectance and transmittance for weakly absorbing samples. There is no fundamental physical or computational reason for this, but apparently there is such an interplay between n and k in the expressions that a large number of combinations may be fitted with essentially the same accuracy to a given experimental pair of reflectance and transmittance values. Thus, it has not been possible to achieve the same level of analysis for $ReSi_2$ as for $CrSi_2$. Earlier this year we found the same problem with the optical analysis of $IrSi_{1.75}$ thin films. (The iridium silicide could be grown only as very thin films, and only on 1-1-1 wafers.)

The electrical resistivity of $ReSi_2$ is shown as a function of temperature in Figure 16. The material apparently is in the intrinsic regime, with the data exhibiting a thermal activation energy of ~0.09 eV. Above 670K (1000/T = 1.5), substrate shorting commences as the oxide becomes sufficiently conductive and the apparent activation energy approaches that of intrinsic

silicon, 0.55 eV.

According to basic semiconductor band theory, the intrinsic resistivity activation energy should be half the bandgap [13]. Thus we estimate a forbidden energy gap of 0.18 eV for this material, which is in rough agreement with the optical data of Figure 15.

Our results on $ReSi_2$ contradict a most recent theoretical investigation of the material in which a metallic band structure was predicted [14]. Using fully relativistic pseudopotentials, the energy bands, density of states, and Fermi surface were calculated. It was claimed that the conductivity of $ReSi_2$ should be larger by far than that of $MoSi_2$ or WSi_2. On the other hand, the transparency and thermally activated resistivity we have observed show unequivocally that the material is a narrow bandgap semiconductor. Further research on $ReSi_2$ film formation is needed in order to obtain samples adequate for detailed optical characterization such as was achieved for $CrSi_2$.

Summary and Conclusions; Phase II Research

$CrSi_2$ was found to possess an indirect forbidden energy gap of slightly less than 0.31 eV. Both forms of $LaSi_2$ are metallic conductors and hence merit no further consideration as intrinsic semiconductor infrared detector materials. $ReSi_2$ apparently has a gap of ~0.18 eV; difficulties with thin film formation prevented a detailed optical analysis of the material.

We find that $CrSi_2$ and $ReSi_2$ are interesting candidates for development as intrinsic infrared detector materials. Because these materials are grown directly on silicon substrates, they are particularly interesting for the development of fully integrated optical detectors. The fabrication of focal plane arrays of intrinsic semiconductor detectors made within films of $CrSi_2$ or

$ReSi_2$ should be a straightforward extension of present techniques for making PtSi and Pd_2Si Schottky barrier detector arrays.

In other research we have optically characterized thin films of semiconducting $MnSi_{1.7}$. This material, being quite similar to $CrSi_2$ optically, is a very strong absorber and possesses an indirect gap of slightly less than 0.54 eV. Thus, the absorption edge at ~2.3 microns makes it suitable for use with the window of atmospheric transparency at 2.0 - 2.6 microns and shorter wavelengths.

Phase II research should focus on improved materials preparation, and on the effects of defects on the transport and photoelectronic properties. Recent articles have described the epitaxial growth of the chromium [15] and manganese silicides [16], but the single-crystal regions of the films were of limited size.

The heart of a Phase II research program should be the exploration of epitaxial growth by molecular beam epitaxy. The effects of defects should be investigated with careful materials characterization coupled with mobility measurements (e.g. Hall effect) and lifetime measurements (e.g. photoconductivity). With this knowledge base it should be possible to move with confidence into the area of device development. This may include research on insulators, doping processes, contacts, and patterning of the materials. The research will pay enormous dividends if the semiconducting silicides make it possible to achieve, in a practical way, a new family of integrated infrared detectors on silicon.

Our Phase I research has shown that the semiconducting silicides as a class of materials merit further investigation for use in the integration of optical detectors with silicon-based microelectronics.

References

1. The targets were fabricated by Varian Specialty Metals, Grove City, OH, and of the following purity: Cr (99.85%), La (99.9%), Re (99.9%).

2. Obtained from Monsanto Co., Dallas, TX.

3. M.-A. Nicolet and S.S. Lau, "Formation and Characterization of Transition-Metal Silicides," in VLSI Electronics Microstructure Science, Vol. 6, ed. by N.G. Einspruch and G.B. Larrabee (Academic Press, New York, 1983), Chap. 6.

4. M.C. Bost and J.E. Mahan, "Optical Properties of Semiconducting Iron Disilicide Thin Films," J. Appl. Phys. 58(7), 2696 (1985).

5. J.E. Nestell and R.W. Christy, "Derivation of Optical Constants of Metals from Thin-Film Measurements at Oblique Incidence," Appl. Opt., Vol 11, No. 3, 643 (1972).

6. Powder Diffraction Data File, Card 12-696 (American Society for Testing Materials, Philadelphia, PA).

7. Tetragonal peak positions obtained from Ref. 6, Card 6-047; orthorhombic peak positions calculated from the crystal structure data in Ref. 3.

8. Calculated from the crystal structure data in Ref. 3.

9. H.E. Bennett and J.O. Porteus, "Relation Between Surface Roughness and Specular Reflectance at Normal Incidence", J. Opt. Soc. Am., Vol. 5, No. 2, 127 (1961).

10. O.S. Heavens, Optical Properties of Thin Solid Films (Academic, New York, 1955), p. 114.

11. J.S. Pankove, Optical Processes in Semiconductors (Dover, New York, 1971), Chap. 3.

12. We have heard over the "grapevine" that workers at AT&T Bell Labs have tried, and were unsuccessful, to fabricate $ReSi_2$ thin films.

13. R.A. Smith, Semiconductors, Second Ed. (Cambridge University Press, Cambridge, 1978), Chap. 10.

14. B.K. Bhattacharyya, D.M. Bylander, and L. Kleinman, "Fully Relativistic Energy Bands and Cohesive Energy of $ReSi_2$," to be published.

15. F.Y. Shiau, H.C. Cheng, and L.J. Chen, "Epitaxial Growth of $CrSi_2$ on (111) Si," Appl. Phys. Lett. 45(5), 524 (1984).

16. Y.C. Lian and L.J. Chen, "Localized Epitaxial Growth of $MnSi_{1.7}$ on Silicon," Appl. Phys. Lett. 48(5), 359 (1986).

Figure Captions

1. X-ray diffraction pattern for a representative $CrSi_2$ film grown on a 1-0-0 silicon wafer.

2. X-ray diffraction pattern for tetragonal (a) and orthorhombic (b) $LaSi_2$ films grown on 1-0-0 silicon wafers.

3. X-ray diffraction pattern for a representative $ReSi_2$ film grown on a 1-1-1 silicon wafer.

4. Auger electron spectrum for a representative $CrSi_2$ thin film.

5. Auger electron spectrum for a representative $LaSi_2$ thin film.

6. Auger electron spectrum for a representative $ReSi_2$ thin film.

7. SEM top view (a) and fracture cross-section (b) for a $CrSi_2$ film.

8. SEM top view (a) and fracture cross-section (b) for a $LaSi_2$ film.

9. SEM top view (a) and fracture cross-section (b) for a $ReSi_2$ film.

10. Optical properties of four $CrSi_2$ samples.

11. Optical absorption coefficient of $CrSi_2$, obtained from the data of Figure 10. The four symbols correspond to the four samples of Figure 10.

12. Absorption coefficient data for $CrSi_2$ plotted in a manner appropriate for an indirect gap.

13. Absorption coefficient data for $CrSi_2$ that suggests the occurrence of direct transitions above the band edge.

14. Electrical resistivity as a function of temperature for tetragonal (a) and orthorhombic (b) $LaSi_2$.

15. Optical properties of three $ReSi_2$ films of the following thicknesses: • 768 A, o 461 A, and + 307 A.

16. Electrical resistivity versus reciprocal temperature for $ReSi_2$; solid lines correspond to the activation energies shown.

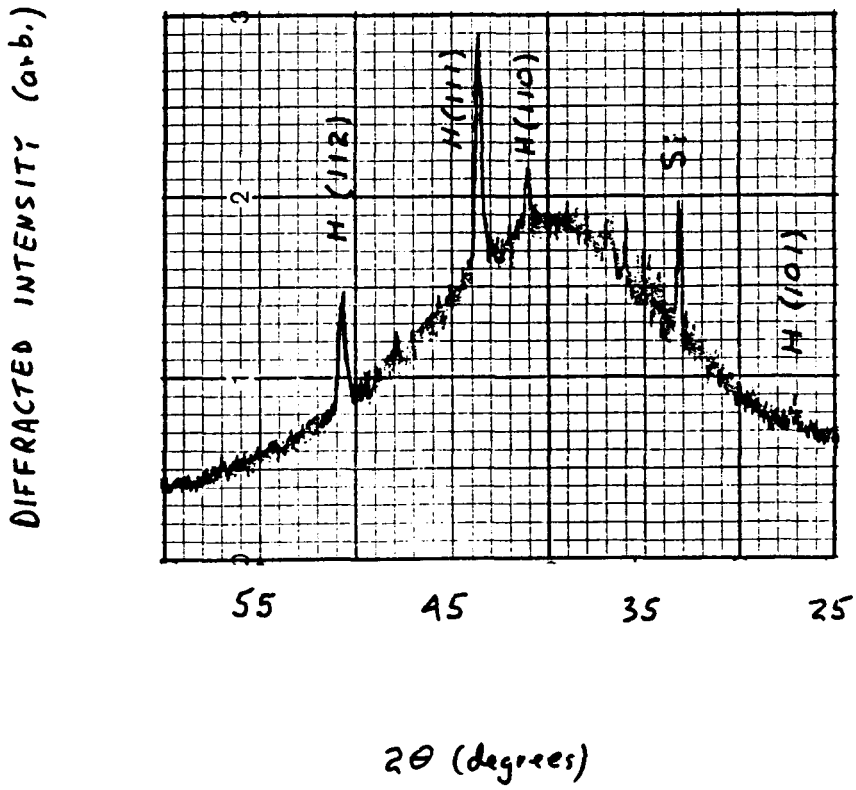
DIFFRACTED INTENSITY (a.b.)
3
2
1
H (112)
H (111)
H (110)
Si
H (101)
55
45
35
25
2θ (degrees)

Fig. 1

Fig. 2

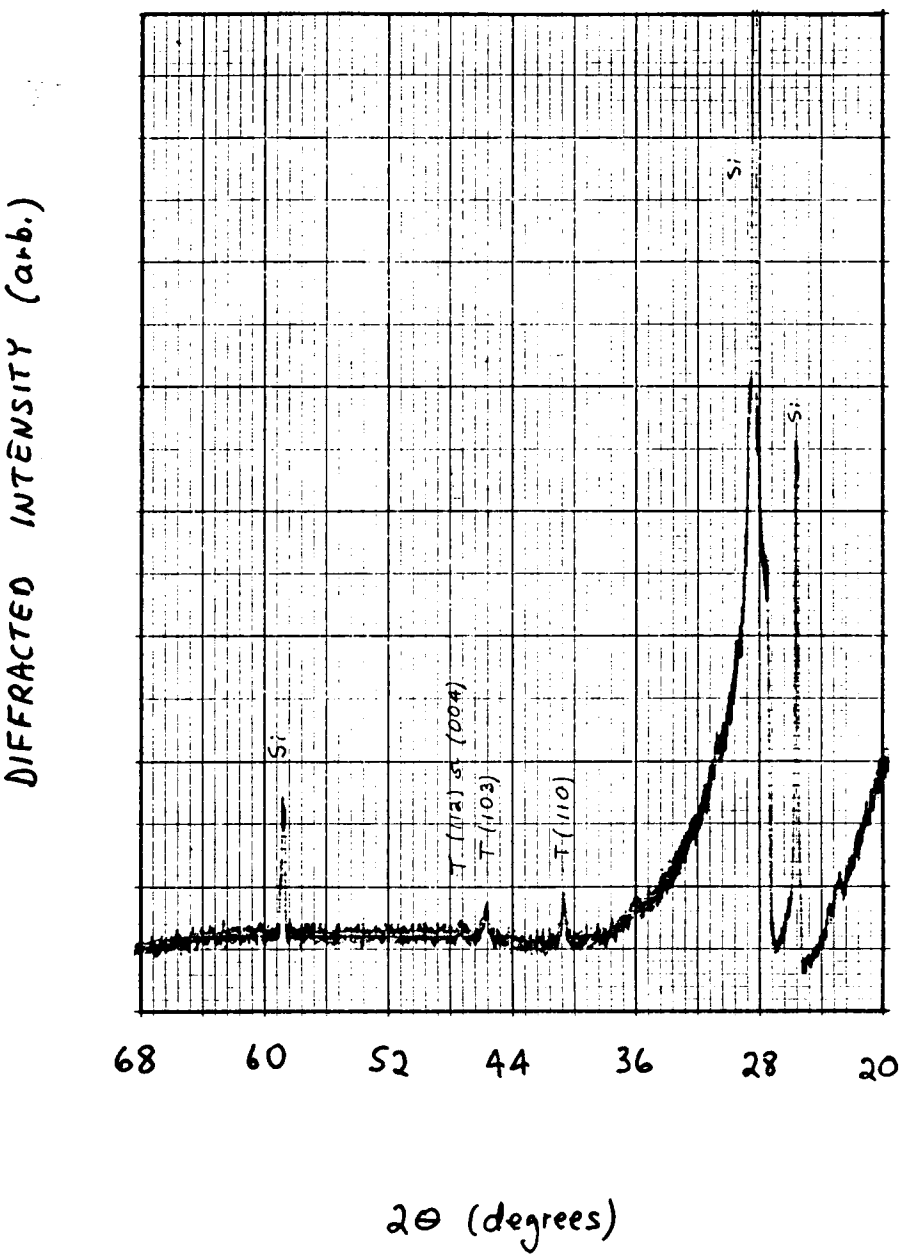
DIFFRACTED INTENSITY (a.b.)
Si
T (112) or (004)
T (103)
T (110)
Si
Si
68
60
52
44
36
28
20
2θ (degrees)

Fig. 3

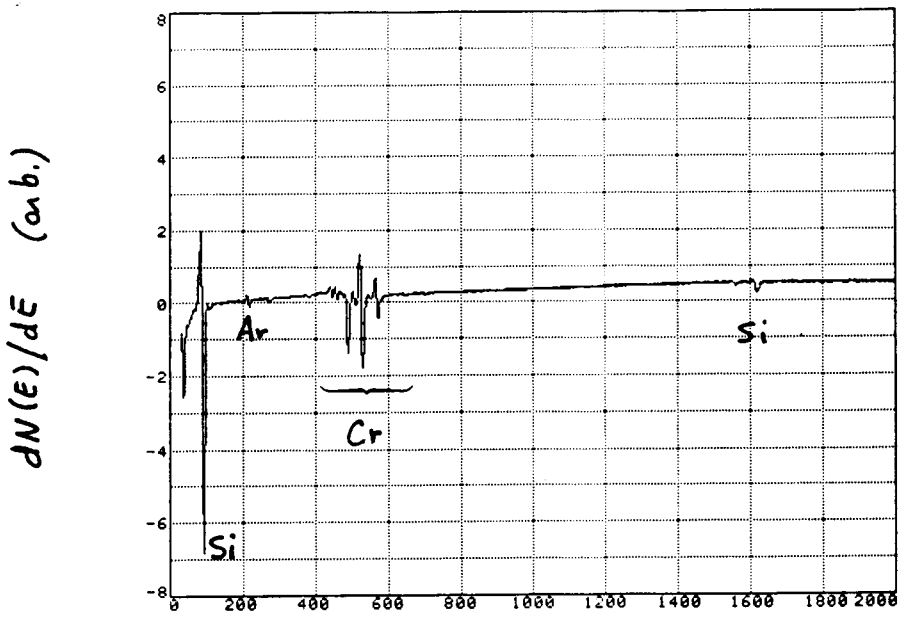
dN(E)/dE (arb.)
8
6
4
2
0
-2
-4
-6
-8
0
200
400
600
800
1000
1200
1400
1600
1800
2000
Ar
Cr
Si
Si
KINETIC ENERGY (eV)

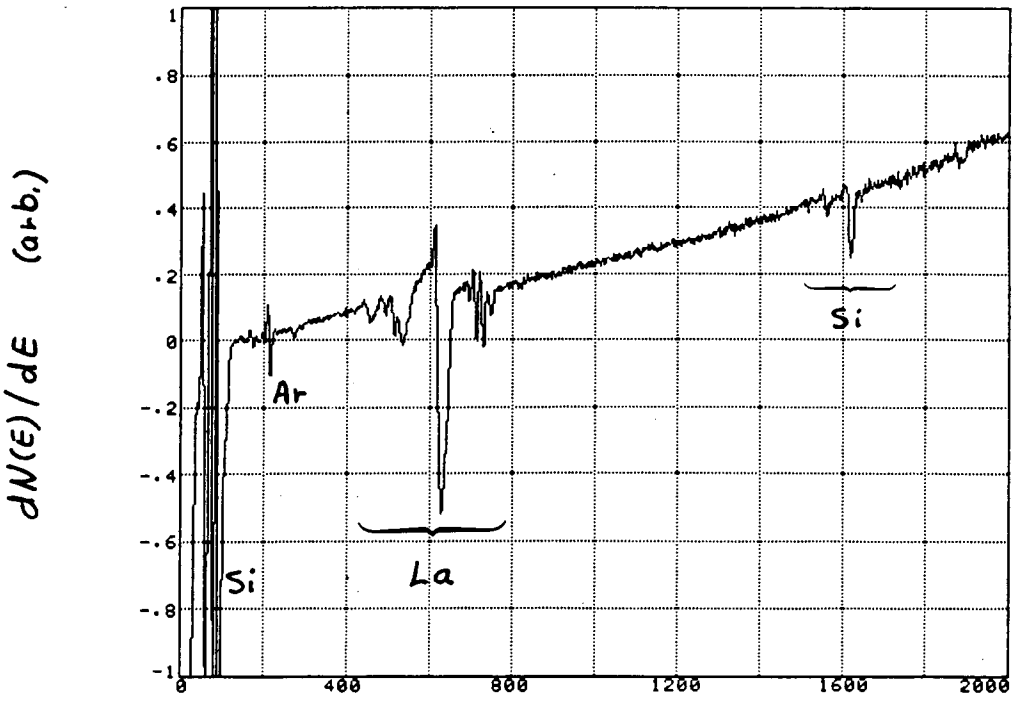
dN(E)/dE (arb.)
1
.8
.6
.4
.2
0
-.2
-.4
-.6
-.8
-1
0
400
800
1200
1600
2000
Ar
Si
La
Si
KINETIC ENERGY (eV)

Fig. 5

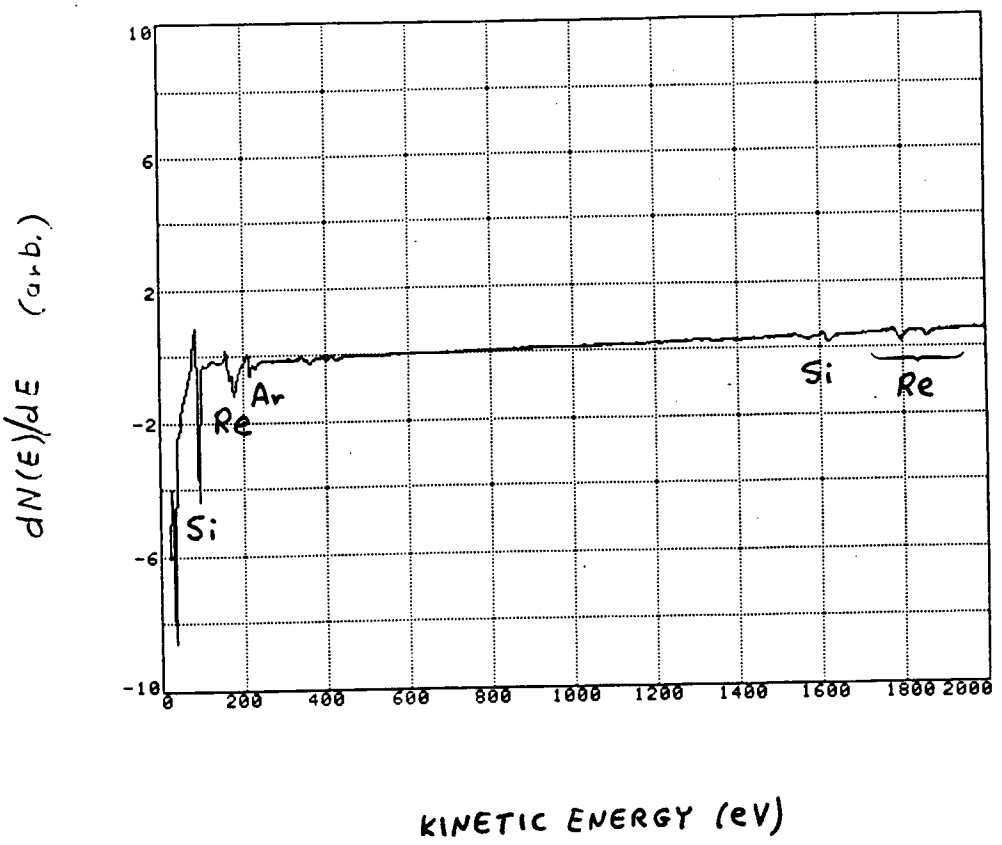
dN(E)/dE (arb.)
10
6
2
-2
-6
-10
0
200
400
600
800
1000
1200
1400
1600
1800
2000
Si
Re
Ar
Si
Re
KINETIC ENERGY (eV)

Fig. 6

ORIGINAL PAGE
BLACK AND WHITE PHOTOGRAPH

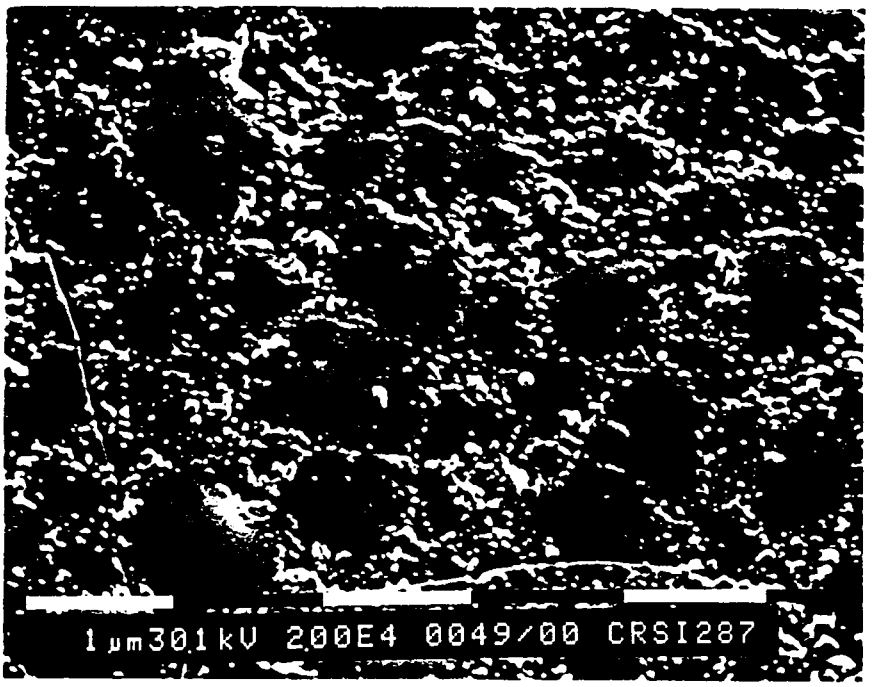

(a)

(b)

Fig. 7

ORIGINAL PAGE
BLACK AND WHITE PHOTOGRAPH

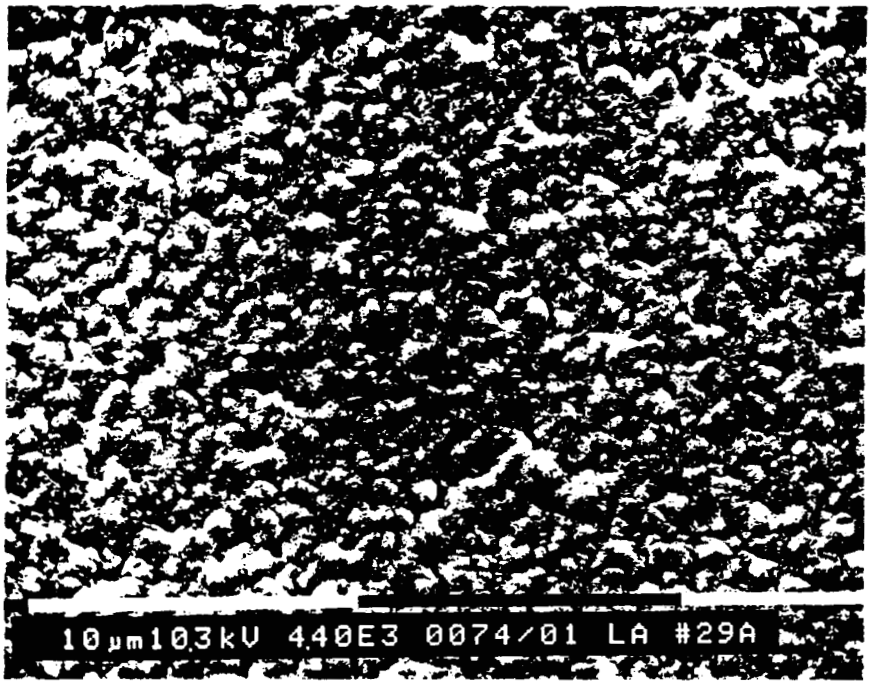

(a)

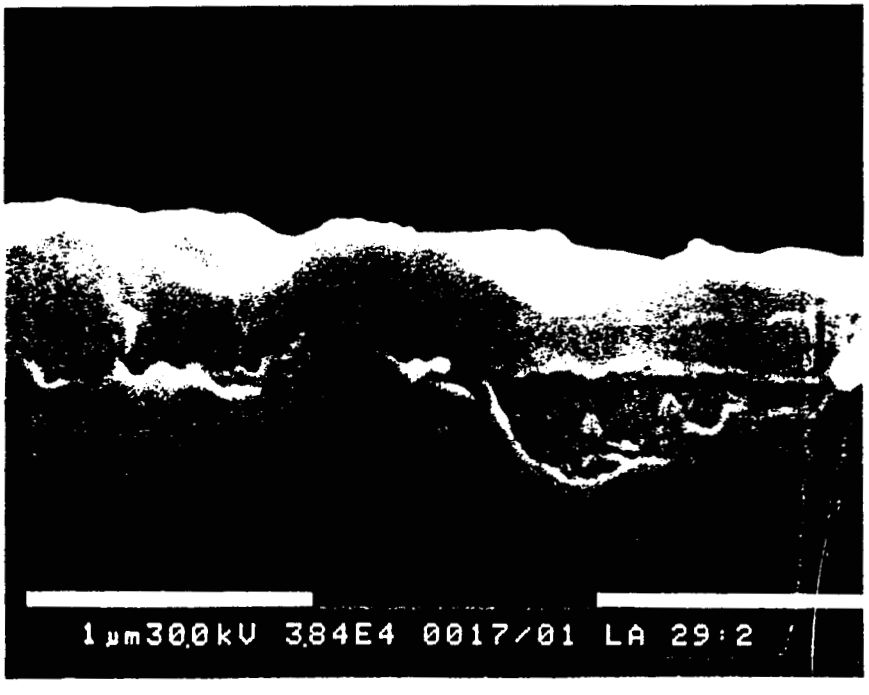

(b)

Fig. 8

ORIGINAL PAGE
BLACK AND WHITE PHOTOGRAPH

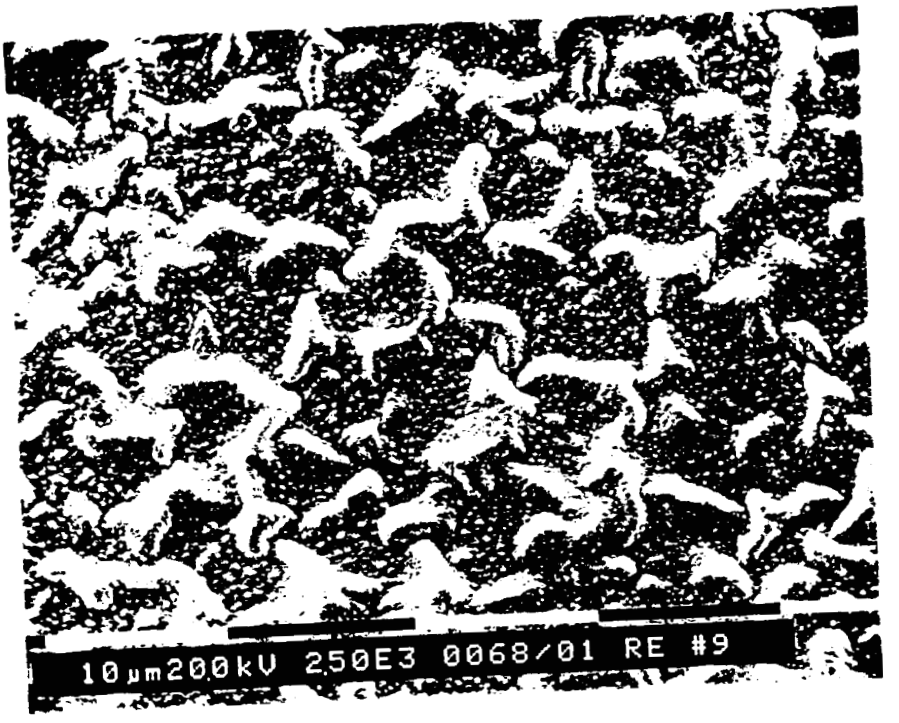

(a)

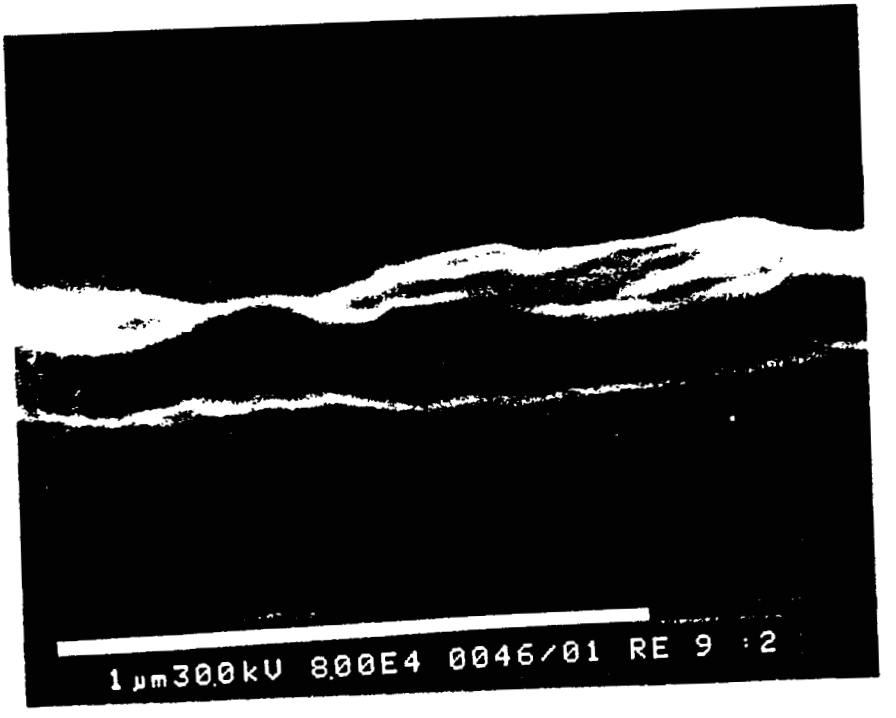

(b)

Fig. 1

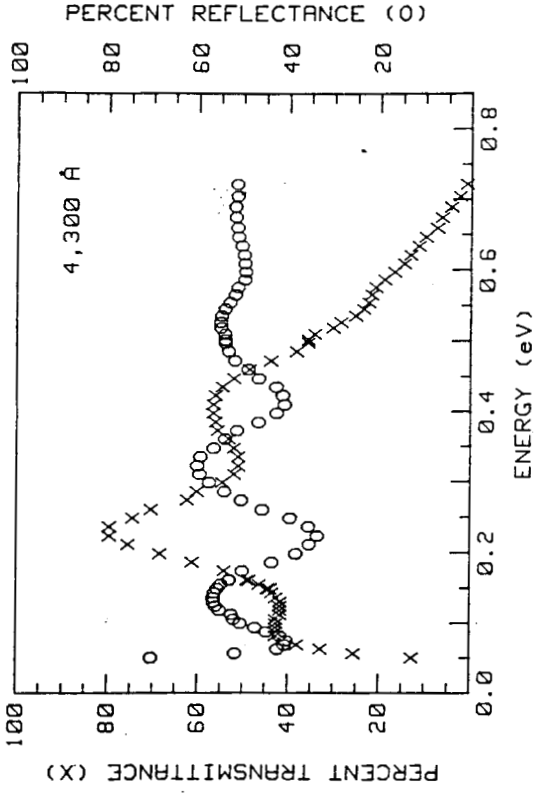
PERCENT REFLECTANCE (O)
4,300 Å
PERCENT TRANSMITTANCE (X)
ENERGY (eV)

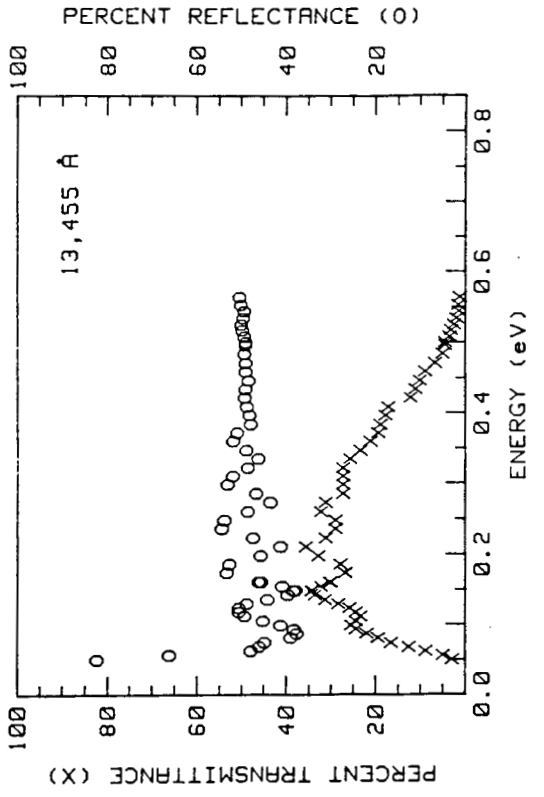
PERCENT REFLECTANCE (O)
13,455 Å
PERCENT TRANSMITTANCE (X)
ENERGY (eV)

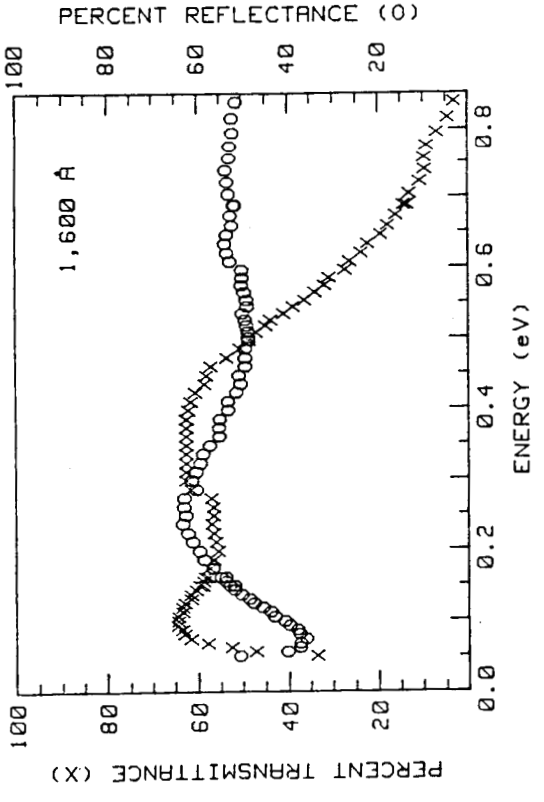
PERCENT REFLECTANCE (O)
1,600 Å
PERCENT TRANSMITTANCE (X)
ENERGY (eV)

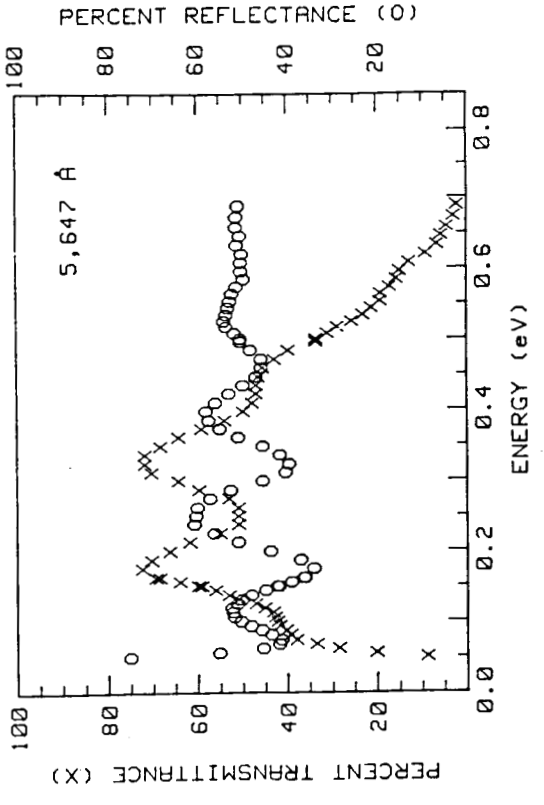
PERCENT REFLECTANCE (O)
5,647 Å
PERCENT TRANSMITTANCE (X)
ENERGY (eV)

Fig. 10

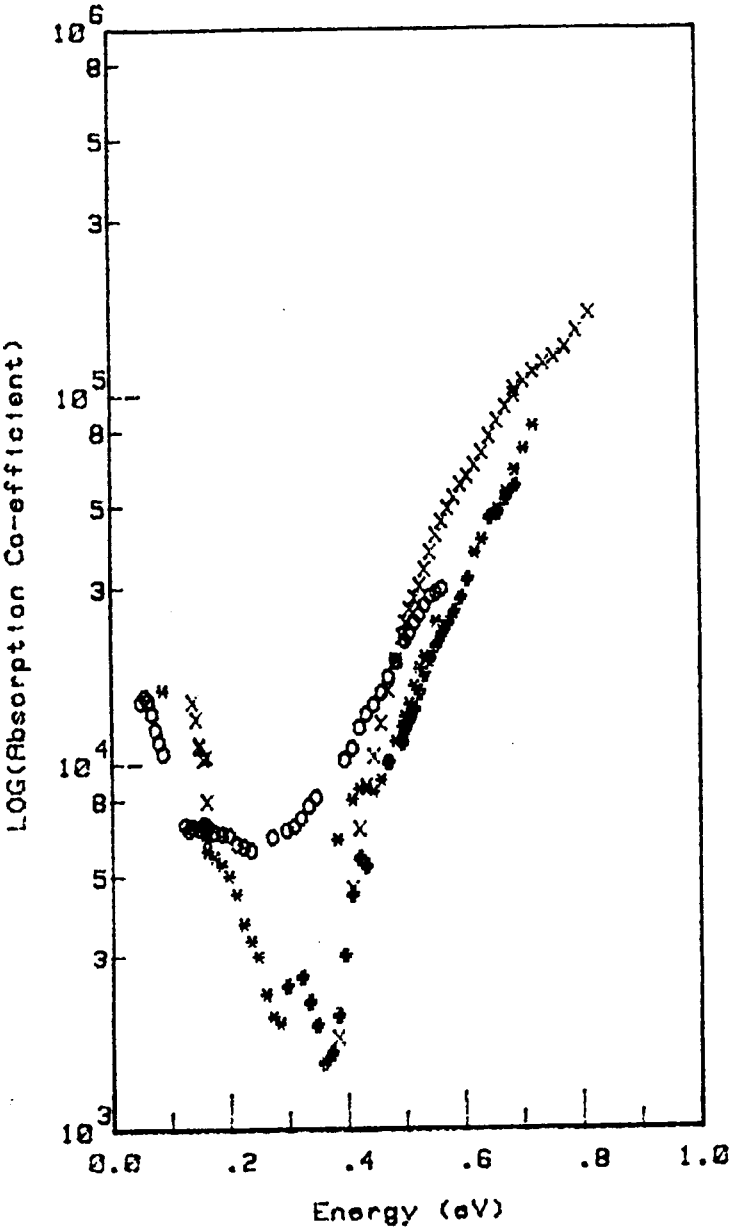
LOG(Absorption Co-efficient)
10^6
8
5
3
10^5
8
5
3
10^4
8
5
3
10^3
0.0
.2
.4
.6
.8
1.0
Energy (eV)

Fig. 11

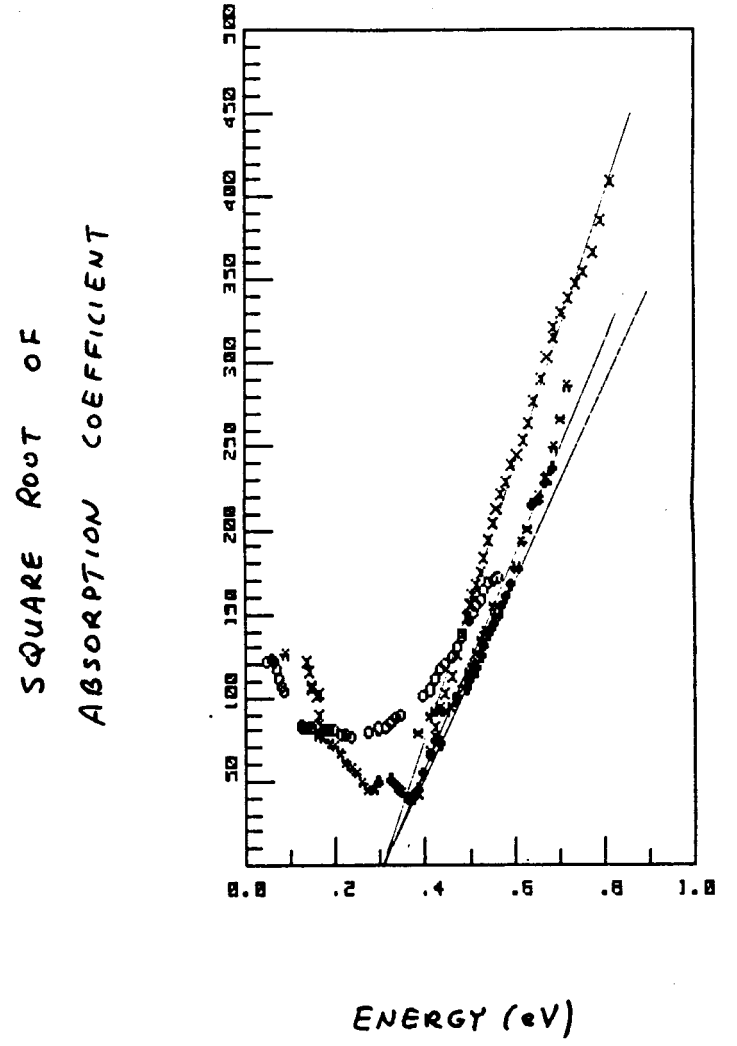
SQUARE ROOT OF
ABSORPTION COEFFICIENT
50
100
150
200
250
300
350
400
450
500
0.0
.2
.4
.6
.8
1.0
ENERGY (eV)

Fig. 12

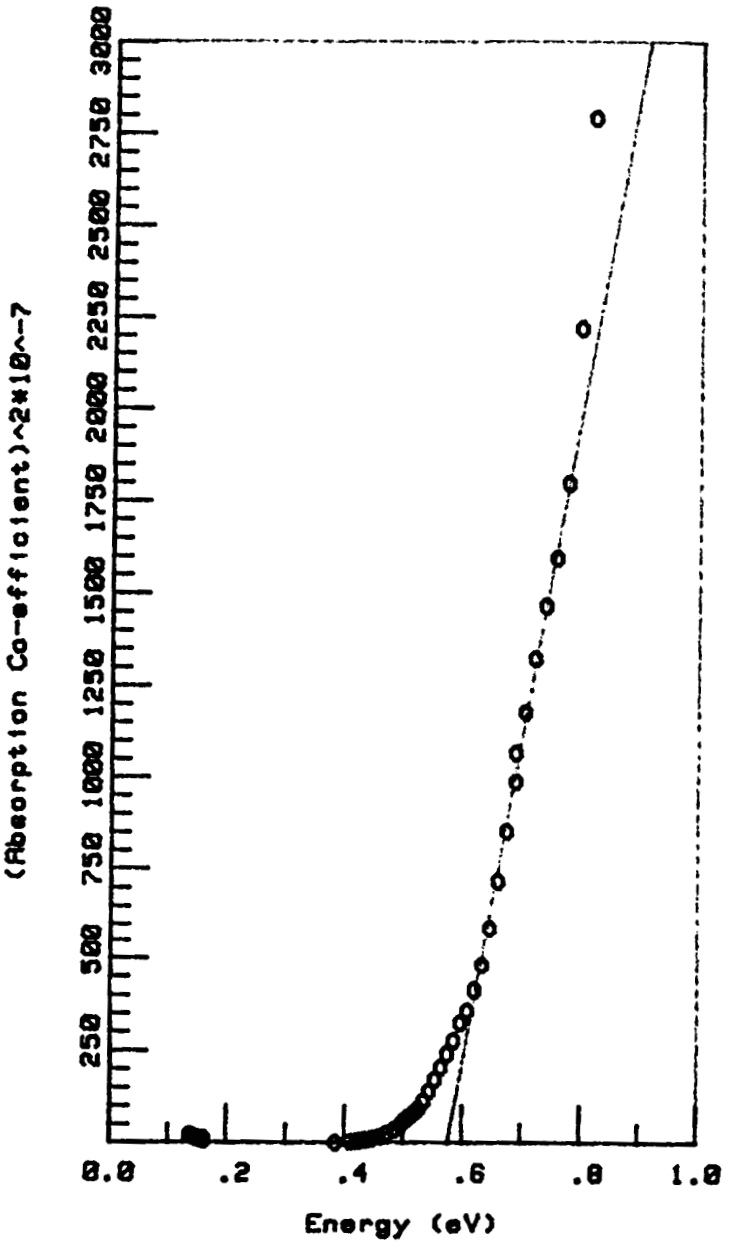
(Absorption Co-efficient)^2*10^-7
250
500
750
1000
1250
1500
1750
2000
2250
2500
2750
3000
0.0
.2
.4
.6
.8
1.0
Energy (eV)

Fig, 13

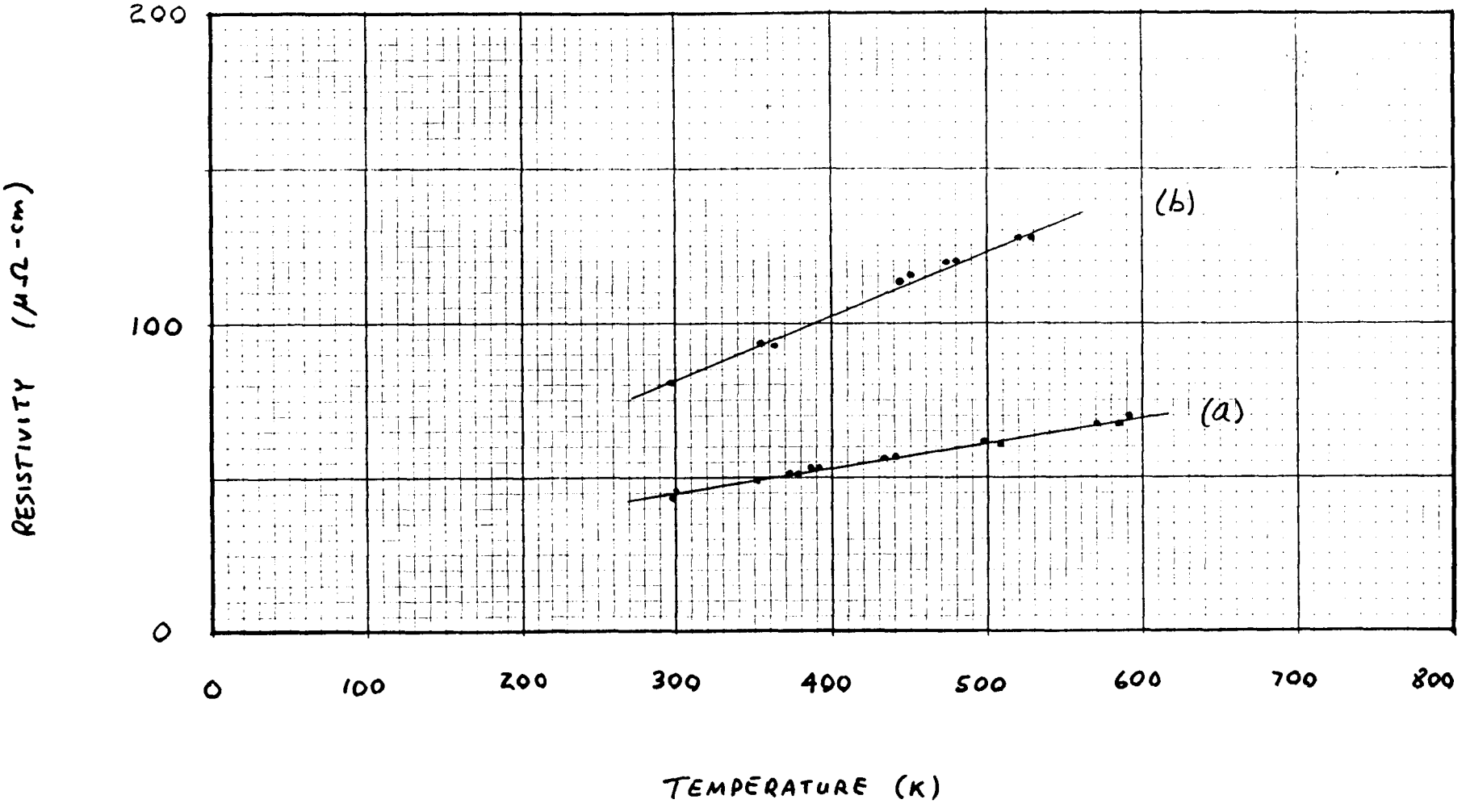
200
100
0
0
100
200
300
400
500
600
700
800
(b)
(a)
RESISTIVITY (μΩ-cm)
TEMPERATURE (K)

Fig. 14

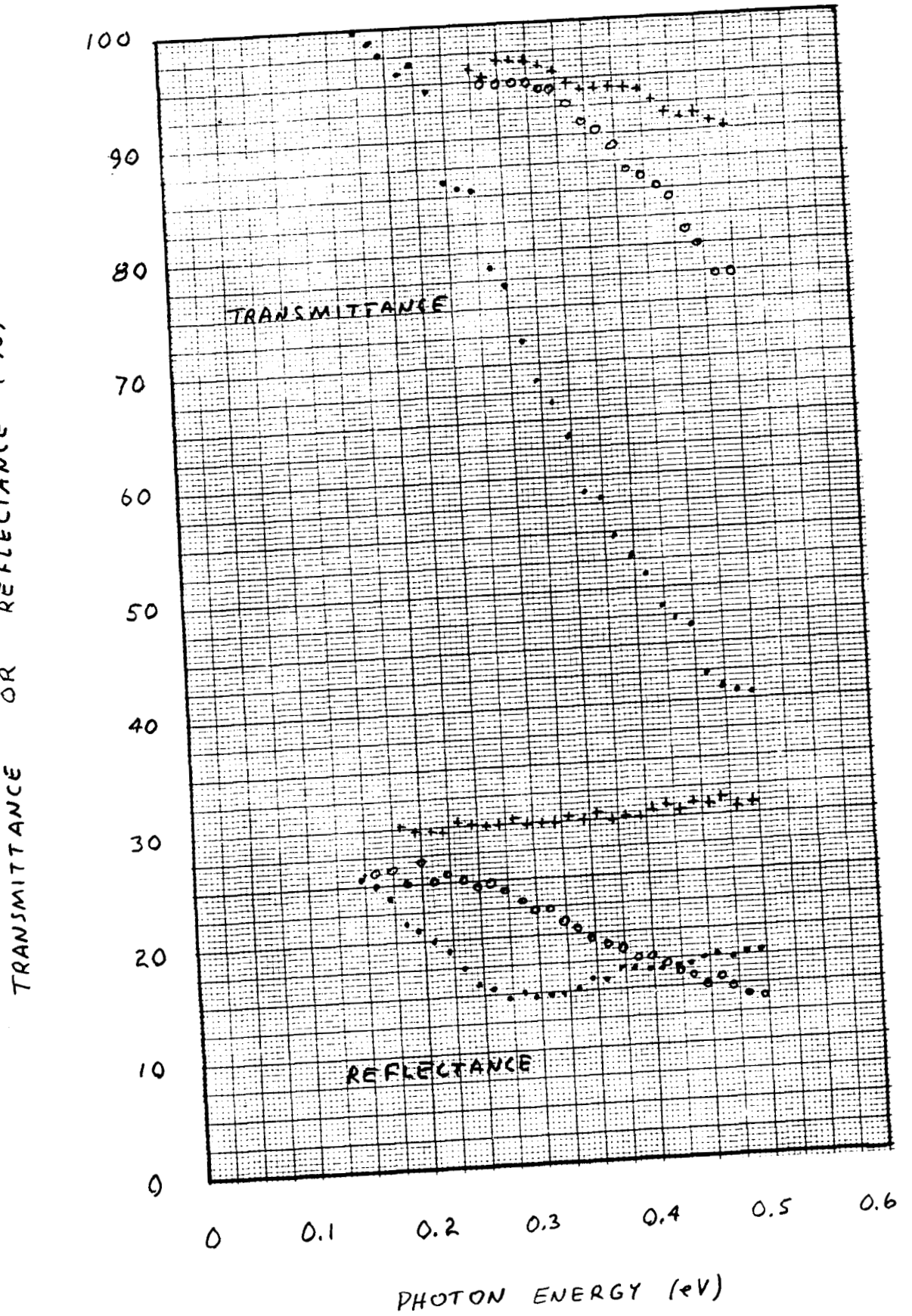
100
90
80
70
60
50
40
30
20
10
0
TRANSMITTANCE
REFLECTANCE
0
0.1
0.2
0.3
0.4
0.5
0.6
TRANSMITTANCE OR REFLECTANCE (%)
PHOTON ENERGY (eV)

Fig. 15

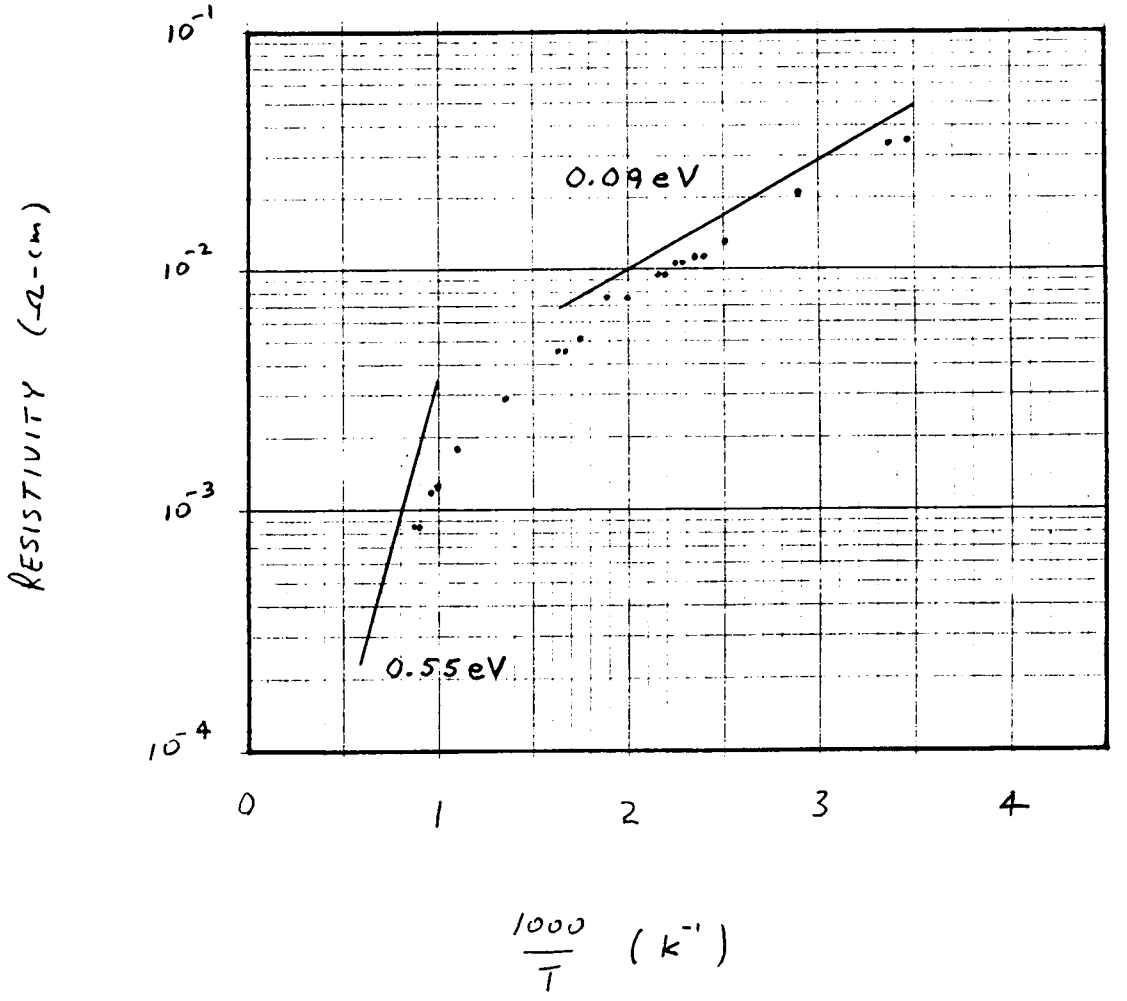

Fig. 16